(Received 24 February 2025, Accepted 2 April 2025, Scheduled 7 April 2025)

Compact Physical and Electrical Patch Antenna Engineered for 5G Mobile Devices and Multiband Systems

Nazrin Haziq Jemaludin[1], Ahmed Jamal Abdullah Al-Gburi[1,*], Muhannad K. Abdulhameed[2,3], Sarah R. Hashim[4], Dunya Zeki Mohammed[5], Tale Saeidi[6], Anupma Gupta[7], Zahriladha Zakaria[1], Nurhayati Nurhayati[8], and Rania Hamdy Elabd[9]

[1]*Center for Telecommunication Research & Innovation (CeTRI)*
Fakulti Teknologi Dan Kejuruteraan Elektronik Dan Komputer (FTKEK)
Universiti Teknikal Malaysia Melaka (UTeM), Jalan Hang Tuah Jaya, 76100, Durian Tunggal, Melaka, Malaysia
[2]*Computer Scince Department, University of Kerbala, Karbala, Iraq*
[3]*Air Conditioning Engineering Department, Faculty of Engineering, Warith Al-Anbiyaa University, Iraq*
[4]*Department of Cyber Security, Al-Zahraa University for Women, Karbala, Iraq*
[5]*Department of Electronic and Communications Engineering, Gilgamesh University, Baghdad, Iraq*
[6]*WiSAR Lab, Atlantic Technological University (ATU), Letterkenny, Co. Donegal F92 FC93, Ireland*
[7]*Department of Electronics and Communication Engineering, Saveetha School of Engineering*
Saveetha Institute of Medical and Technical Sciences, Thandalam, 602105, Chennai, Tamilnadu, India
[8]*Department of Electrical Engineering, Universitas Negeri Surabaya, Surabaya 60231, Indonesia*
[9]*Department Electronic and Communication, Higher Institute of Engineering and Technology in New Damietta, Damietta, Egypt*

ABSTRACT: This article presents a compact multi-band microstrip patch antenna designed for 5G, Ku, and K-band applications. The antenna operates at 3.5 GHz and 15.6 GHz, supporting 5G communications (3.3–3.6 GHz) and satellite applications (15.6–20 GHz). Fabricated on an FR4 substrate ($\varepsilon r = 4.3$, $\tan\delta = 0.025$) with dimensions of $13 \times 10 \times 1.6\,\text{mm}^3$ ($0.15\lambda_o \times 0.12\lambda_o \times 0.02\lambda_o$), where λ_o represents the wavelength at the lower frequency of 3.5 GHz, the antenna achieves return losses of -19 dB and -39 dB at the respective frequencies, with peak gains of -2.8 dBi and 3.7 dBi. The design's consistency is validated through a comparative analysis with recent studies. The antenna was placed near the ear and mouth area of a human head phantom model to perform a comprehensive SAR analysis. SAR analysis confirms compliance with safety standards, maintaining SAR levels below 2 W/kg. The proposed design demonstrates promising performance for modern communication systems.

1. INTRODUCTION

Smartphones have transformed personal computing and mobile communication. By combining the core functions of traditional mobile phones with advanced computing capabilities, these devices enable users to perform tasks far beyond basic text messaging and phone calls. Featuring touchscreens, high-resolution cameras, GPS navigation, and a wide range of applications. Smartphones facilitate multimedia use, social media engagement, and web browsing, revolutionising how individuals interact with technology [1–4]. The evolution from basic mobile phones to advanced smartphones has been facilitated by technological advancements, including improved connectivity options like 4G and 5G networks, extended battery life, and enhanced processing power [5–7]. As smartphones continue to evolve, they are becoming indispensable tools for both personal and professional uses, enabling users to efficiently manage their lives from the palm of their hand.

Figure 1 illustrates that conventional mobile terminal antenna designs can be categorized into loop antennas, monopole antennas, inverted-F antennas (IFAs)/planar inverted-F antennas (PIFAs), monopole slot antennas, and composite right/left-handed (CRLH)-inspired antennas. Beyond these conventional designs, reconfigurable antennas, particularly those with frequency-reconfigurable capabilities, are often employed in mobile terminal antenna development to improve impedance bandwidth. For MIMO applications, antennas with polarisation

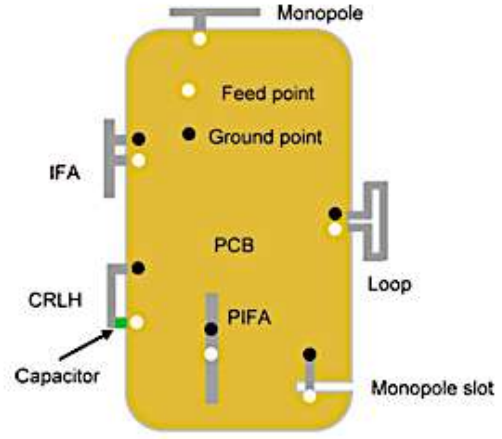

FIGURE 1. Conventional antenna designs for mobile terminals.

* Corresponding author: Ahmed Jamal Abdullah Al-Gburi (ahmedjamal@ieee.org).

characteristics and programmable patterns are also receiving a lot of research.

The accelerated advancement of wireless communication technologies has generated an extraordinary demand for high-performance antennas, particularly for 5G networks and future generations. The need for compact, efficient, and scalable antennas has become increasingly critical as mobile devices play an ever more integral role in daily life [8, 9]. Most modern smartphones now support 5G networks, offering enhanced bandwidth, reduced latency, and faster speeds to enable seamless voice calls and mobile data services, effectively meeting the demands of everyday communication [10].

The growing demand for compact and efficient communication solutions has increased the prominence of patch antennas in smartphone design. As mobile devices continue to evolve to support advanced technologies such as 5G, integrating antennas that deliver high performance within limited space has become a significant challenge [11]. Printed circuit boards (PCBs) are seamlessly integrated with microstrip antennas, which are highly favored for their lightweight and slim profile. However, achieving optimal performance parameters — such as bandwidth, gain, and efficiency — while maintaining a compact size presents significant design challenges. Patch antennas offer several advantages, including a lightweight and low-profile design; however, they also face technical challenges such as impedance matching, bandwidth optimisation, and radiation efficiency. Addressing these challenges is crucial for manufacturers to achieve a balance between functionality and miniaturisation, ensuring reliable connectivity without compromising the device's aesthetics or performance [12, 13]. This paper explores recent advancements in patch antenna technology, highlighting innovative design strategies that enable seamless integration into modern smartphones while tackling these critical challenges.

In [14], a monopole antenna is introduced that operates in a single band (3.5 GHz WiMAX) when being inactive. When being activated, it transitions to dual-band functionality, supporting Wi-Fi operating at 2.45 GHz and 5.2 GHz band. The antenna's efficiency, measured at 86%, 93.5%, and 84.4% at 2.45 GHz, 3.5 GHz, and 5.2 GHz, respectively, demonstrates its effectiveness across these frequency ranges. Additionally, its directivity values of 2.13 dBi, 2.77 dBi, and 3.99 dBi further validate its performance. The authors in [15] present an eight-element MIMO antenna for 5G handsets, designed to operate at 3.5 GHz and 5.5 GHz. The mutual coupling values are maintained at -20 dB in the lower frequency band and -22 dB in the upper frequency band. The ECC of each antenna element is less than 0.11, with radiation efficiencies exceeding 68% in the lower band and 78% in the upper band. In [16], a monopole antenna, shaped like the numeral "3," is proposed for wireless laptop applications. The antenna resonates at frequencies of 3.45 GHz and 5.5 GHz with a voltage standing wave ratio (VSWR) of less than 2. The measured impedance bandwidth for the lower band spans 20% (3.21–3.91 GHz), while the upper band covers 15% (5.05–5.85 GHz). This design supports 5G sub-6 GHz and WLAN functionality. In [17], a triband Vivaldi antenna has been designed to operate at frequencies of 3.8 GHz, 5.2 GHz, and 8 GHz, offering bandwidths of 1.6 GHz, 1.2 GHz, and 1 GHz, respectively. A compact simple planar antenna design measuring $40 \times 15 \times 0.8\,\text{mm}^3$, covering 700–960 MHz and 1600–5500 MHz with $|S_{11}| \leq -6$ dB, suitable for 5G terminals is introduced in [18]. In [19], the authors utilize a flexible PDMS substrate with an impedance bandwidth of 1.225 GHz and a reflection coefficient of -37 dB. Next, the authors in [20] develop a super-compact patch antenna for ultra-wideband (UWB) frequencies. The antenna size was 15 mm $\times$ 17 mm $\times$ 1.54 mm, and it was fabricated using a Rogers RT/duroid 5880 substrate. In [21], the authors present a capacitively-fed antenna design, supporting multiple modes, covering 790–6000 MHz, making it versatile for various wireless standards. The antenna in [22] combines sub-6 GHz and mmWave capabilities, allowing for the efficient use of space within smartphones while maintaining performance across multiple frequency bands. Lastly, researchers in [23] discuss a single-patch antenna designed for 3.5 GHz, suitable for 5G applications, and it utilizes a DGS structure to enhance the bandwidth from 105.1 MHz to 158.4 MHz.

While previous works focus on either compactness or bandwidth, achieving both simultaneously without compromising radiation efficiency remains a critical challenge. This work addresses this gap by introducing a compact multi-band patch antenna that optimally balances size, bandwidth, and gain. Designed for seamless integration into modern smartphones, the proposed antenna effectively supports 5G, Ku-band, and K-band applications while maintaining high performance and safety compliance.

This study presents an innovative compact patch antenna with reliable characteristics, including multiband operation, high gain, well-optimized radiation patterns, and a distinctive geometric design. The proposed antenna is highly suitable for integration into compact electronic devices, providing exceptional versatility for various applications, including 5G, Ku-band, and K-band technologies. It performs operations within two critical frequency ranges: 3.36–3.67 GHz, which has a resonant frequency of 3.5 GHz, and 15.6–20 GHz, which offers a broad bandwidth. The antenna exhibits excellent performance with resonant frequencies at 17.1 GHz, 19.2 GHz, and 3.5 GHz, enabling operation across a broad spectrum, including Ku-band, K-band, and 5G applications. Simulation results demonstrate its effectiveness in terms of reflection coefficients, radiation patterns, and gain within these frequency ranges. Additionally, the study provides a comprehensive Specific Absorption Rate (SAR) analysis and investigates the impact of various antenna parameters under different environmental conditions. The proposed antenna offers a promising solution for a wide range of wireless communication and 5G applications, thanks to its frequency versatility and compact design.

2. ANTENNA CONFIGURATION

In this research, the antenna is designed for optimal performance at 3.5 GHz and at a frequency within the Ku and K-bands, which are essential for 5G communication systems. It also features a rectangular patch design. To create a super-miniaturized multiband antenna, the developed radiating patch

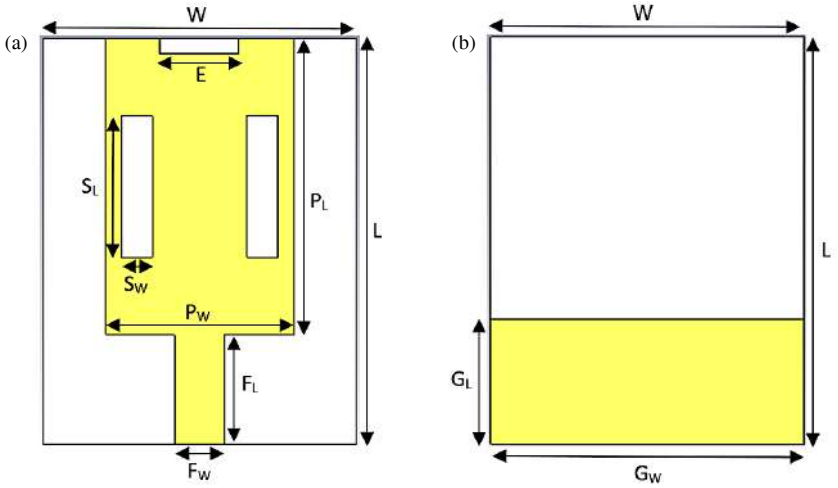

FIGURE 2. (a) Top and (b) Back views of the proposed multiband antenna.

TABLE 1. Design specifications of the antenna.

Parameter	Dimensions (mm)
Substrate Length, L	13
Substrate Width, W	10
Patch Length, PL	9.5
Patch Width, PW	6
Feedline Length, FL	3.5
Feedline Width, FW	1.6
Ground Length, GL	4
Ground Width, GW	10
Rectangular Upper Slot, E	2.5
Slot Length, SL	4.5
Slot Length, SW	1
Substrate Length, L	13

is structured around rectangular radiators. The antenna's feed line consists of a linearly tapered transmission line with low-impedance rectangular outer surfaces that gradually transition to a specific high-impedance level. An FR4 laminate substrate with a thickness of 1.6 mm, a loss tangent of 0.02, and a relative permittivity of 4.3 is used to construct the compact multiband antenna. Figure 2(a) shows the dimensional representation of the proposed design, while Figure 2(b) presents its side view. Table 1 provides a detailed analysis of the dimensional specifications for the proposed multiband antenna.

The substrate characteristics and resonant frequency determine the patch dimensions. The equations presented in Eqs. (1) and (2) from [24] can be used to determine the width and length of the patch:

$$W = \frac{C}{2f_o}\sqrt{\frac{2}{\varepsilon_r+1}} \tag{1}$$

$$L = \frac{C}{2f_o}\sqrt{\frac{2}{\varepsilon_r-1}} \tag{2}$$

This equation defines the speed of light as C, the operating frequency as f_o, and the permittivity value of the substrate as ε_r. The characteristic impedance of the transmission line is the primary factor determining the width of the feedline, typically set at 50 Ω. The feedline width can be calculated using the formula provided in Eq. (3) from [24]:

$$W_F = \frac{2hZ_o}{\varepsilon_r+1} \tag{3}$$

The permittivity value of the substrate is denoted by ε_r, while the characteristic impedance of the transmission line is represented by Z_o. In this context, h refers to the thickness of the substrate. The antenna undergoes simulations during the design phase using CST software to refine several parameters.

2.1. Antenna Design and Geometry

The primary configuration of the antenna design that has been proposed is a rectangular patch placed to a partial ground plane. We select a rectangular patch with a width of 6 mm and a length of 9.5 mm during the initial design phase.

By lowering the ground plane, introducing two symmetrical rectangular slots at the center, and positioning a horizontal slot at the top of the patch, the standard rectangular patch is modified to operate within the 3.5 GHz and 15–20 GHz range, which encompasses the sub-6 GHz, Ku, and K bands. As illustrated in Stage 1 of Figure 3, the conventional rectangular patch antenna is initially designed to resonate at 8 GHz on an FR-4 substrate.

Calculations have been performed to determine the patch dimensions required for the antenna to function at 8 GHz and 18 GHz in Stage 1. A rectangular metal conductor patch, measuring 6 mm × 9.5 mm, is positioned on a 10 mm × 13 mm FR4 substrate, shown in grey. The return loss is approximately 14 dB, and the resonant frequency is around 7.5 GHz, as depicted in Figure 3.

Figure 3 presents the four distinct phases of the antenna design's progression. The initial design, featuring a basic feed structure and a simple rectangular patch, is shown in Stage 1. The reflection coefficient curve (red line) exhibits a significant

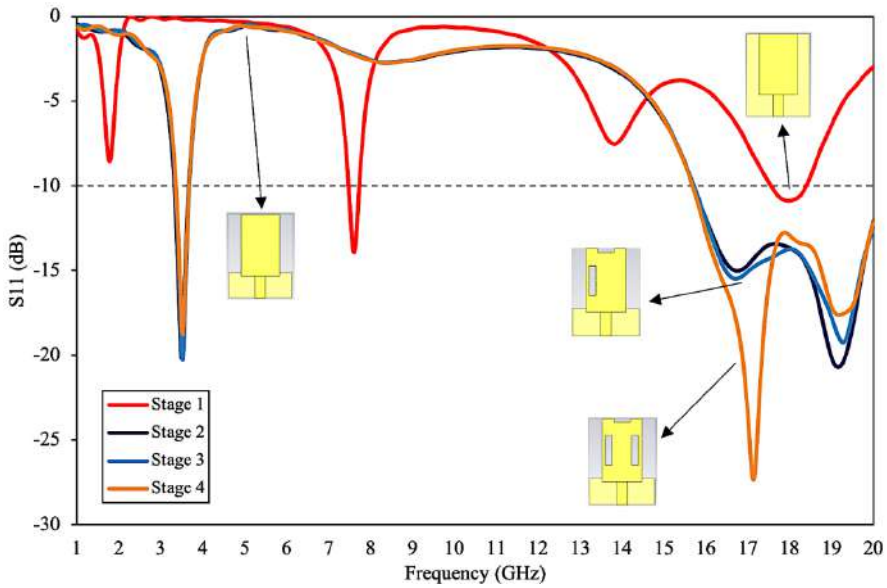

FIGURE 3. Evolution of sub-6 GHz, Ku, and K band antennas and their reflection coefficient curves.

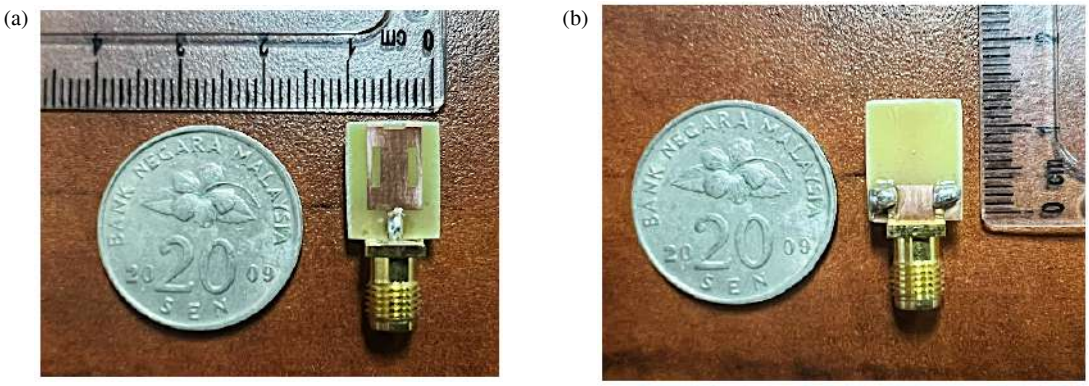

FIGURE 4. Prototype of the proposed antenna.

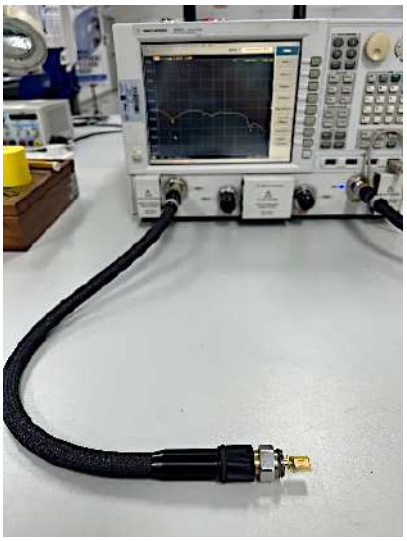

FIGURE 5. Experimental arrangement for characterizing antenna S_{11} parameters via VNA.

drop below -10 dB, indicating that this design primarily supports a single resonant frequency at approximately 7.5 GHz. However, its bandwidth is narrow, and it is unable to effectively accommodate higher frequencies.

The design is modified in Stage 2 to improve bandwidth by incorporating a lower ground structure. A resonance at 3.5 GHz appears, while the reflection coefficient curve (purple line) also displays an additional weak resonance near 17 GHz. Although higher-frequency performance remains underdeveloped, these improvements mark the beginning of multi-band functionality.

Stage 3 introduces slots into the patch, significantly improving the performance of antenna across multiple frequencies. The return loss curve (blue line) now demonstrates stable resonances at 3.5 GHz, 17 GHz, and 19 GHz, all with reflection coefficients at or below -10 dB. These modifications, facilitated by the enhanced current distribution from the slots, enable efficient operation across sub-6 GHz, Ku band, and K band frequencies.

Finally, in Stage 4, the design is optimized for multi-band operation through the addition of more slots and further structural

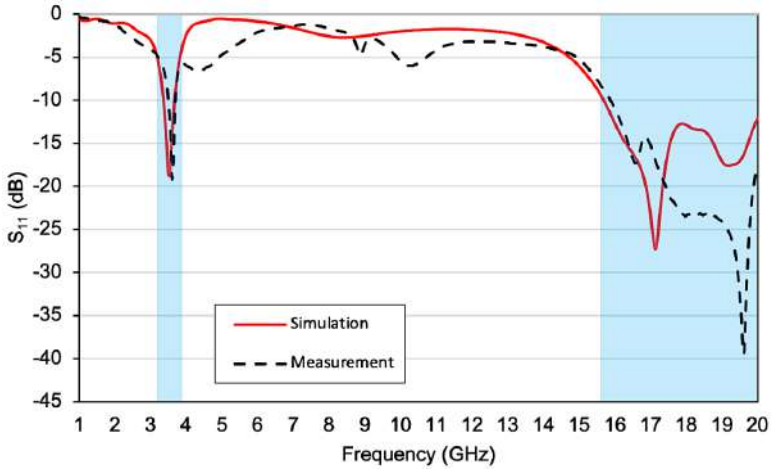

FIGURE 6. Simulated and measured S_{11} (dB) characteristics of the proposed antenna across the frequency spectrum.

refinements. The reflection coefficient curve (black dashed line) reveals resonances at 3.5 GHz, 17 GHz, 19 GHz, and beyond, all of which show reduced reflection losses and strong impedance matching. All the desired resonating frequencies with excellent impedance matching have been successfully achieved. In addition to the 3.5 GHz range, these frequencies include 15.6–20 GHz. The 3.5 GHz resonant frequency also effectively covers the required 100 MHz channel bandwidth. The antenna has achieved optimal multi-band performance, making it highly suitable for sub-6 GHz, Ku band, and K band applications at this stage. This evolution underscores the significant influence of structural modifications on the antenna's electromagnetic performance, resulting in expanded bandwidth and improved efficiency across various frequency bands.

3. RESULTS AND DISCUSSION

The scattering characteristics, radiation pattern, current distribution, and other attributes of the proposed multiband antenna are thoroughly analyzed to assess its performance. The antennas are designed using an FR4 (lossy) substrate material, which has a relative permittivity of 4.3 and a thickness of 1.6 mm. Figure 4 depicts the fabricated antenna.

3.1. S-Parameters

The reflection coefficient of the fabricated antenna was measured using a vector net-work analyzer (VNA), and extensive electromagnetic simulations were performed using CST Studio Suite 2024. Figure 5 shows how the antenna was built up experimentally. Figure 6 demonstrates the performance of a multiband antenna by comparing simulation and measurement results. Significant declines in S_{11} at approximately 3.5 GHz, 17 GHz, and 19 GHz indicate effective impedance matching and efficient power transfer at these resonant frequencies. The antenna's suitability for multiband applications is validated by the strong correlation between simulation (red curve) and measurement (black curve) data, with S_{11} values falling well below -10 dB at the resonant points. Minor discrepancies, particularly at frequencies exceeding 17 GHz, may be attributed to fabrication inaccuracies, material property variations, or measurement setup constraints. The antenna's narrowband behaviour within each frequency range further confirms its multiband functionality. Overall, the findings validate the antenna's effectiveness for wireless communication systems, though minor refinements to the fabrication or measurement processes could improve the alignment between experimental and simulated results.

3.2. Radiation Pattern

The radiation pattern of an antenna, a key performance metric, represents its gain. Gain quantifies the energy intensity radiated in a specific direction compared to an ideal isotropic antenna, which emits energy uniformly in all directions. Directionality, meanwhile, describes the spatial distribution of radiated energy across various directions [24]. Figure 7 shows the radiation patterns demonstrating omnidirectional behavior at the resonant frequencies. Figure 8 illustrates the experimental setup for measuring the antenna's radiation pattern. Figure 9 indicates that the peak gain reaches approximately 2.443 dB.

3.3. Current Distribution

The antenna's current distribution highlights regions of varying current density, indicating potential areas of energy absorption or radiation. This data is essential for refining the antenna's design through modifications to its dimensions or material properties, thereby improving overall performance. Figure 10(a) illustrates a relatively uniform current distribution, with high-intensity regions primarily concentrated around the feedline and specific segments of the antenna structure. This implies that the antenna's resonant behavior at this frequency is characterized by effective energy transfer and moderate radiation in these regions. Meanwhile in Figure 10(b), the distribution of current becomes more localized, with regions of high current density evident near the antenna's edges and slots. The peak value at 3.5 GHz is 359 A/m, meanwhile at 17 GHz it is 316.72 A/m. This suggests that the antenna's performance at a higher resonant frequency is linked to stronger field interactions and potentially greater radiation efficiency at these points.

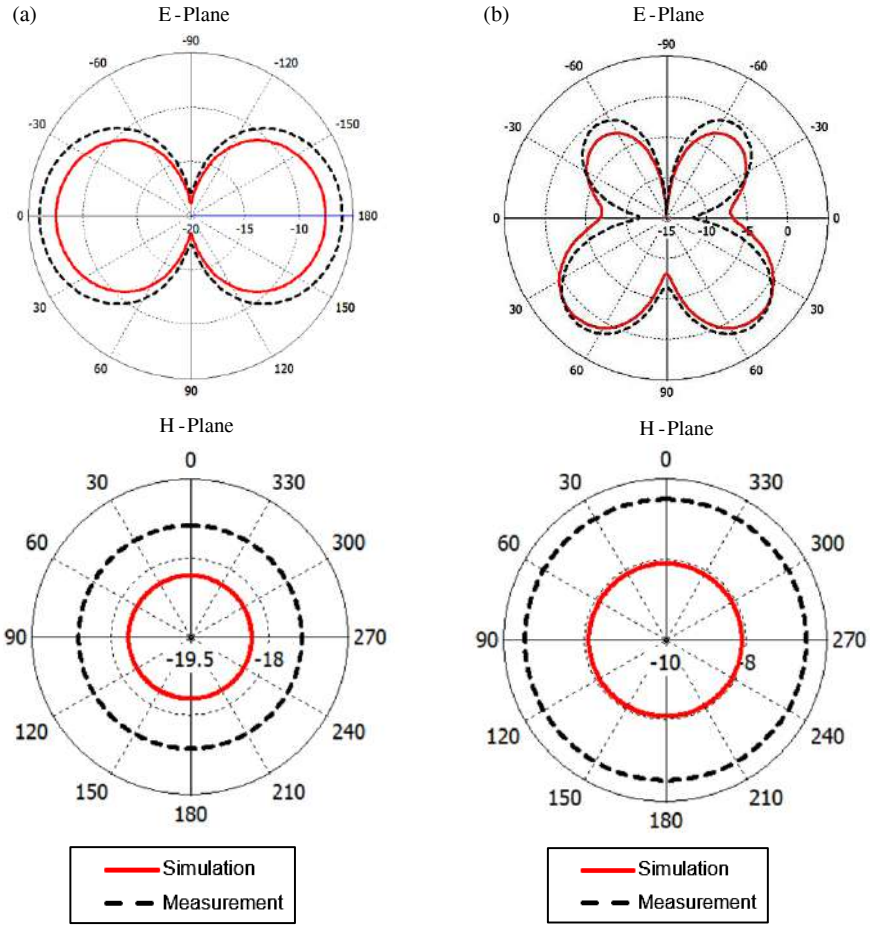

FIGURE 7. Radiation pattern (E and H planes) at (a) 3.5 GHz and (b) 17 GHz.

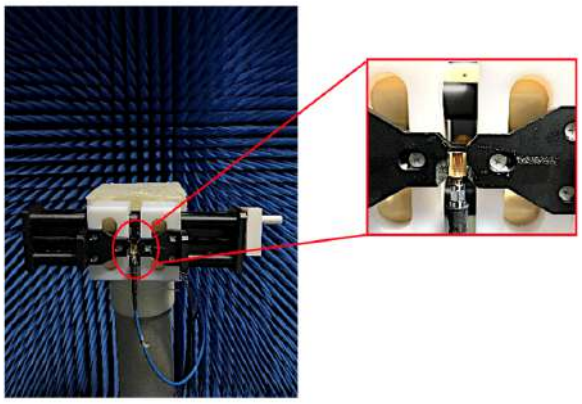

FIGURE 8. Antenna radiation pattern measurement setup.

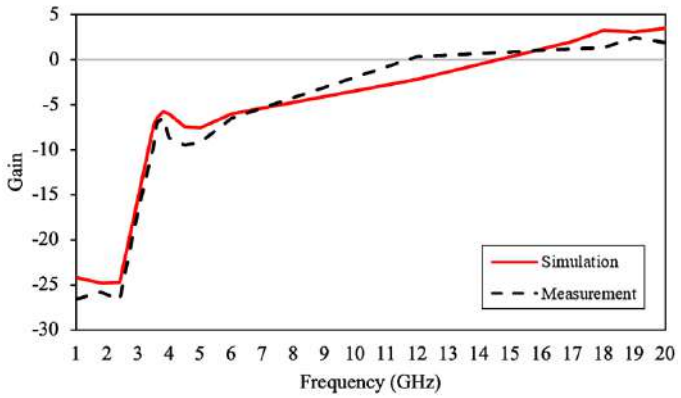

FIGURE 9. The gain pattern of the proposed antenna.

3.4. Compactness Optimization

The antenna's initial purpose was to operate at 3.5 GHz. However, the ground plane was subsequently reduced in size, and numerous integrated modules were incorporated to enable the device to support frequencies of up to 17 GHz. The antenna would have measured 539.15 mm^2 ($0.15\lambda_0 \times 0.12\lambda_0 \times 0.02\lambda_0$) if the design had been exclusively concentrated on 3.5 GHz. However, at the upper frequency of 17 GHz, it occupies only 42.75 mm^2, achieving a 92.07% improvement in compactness.

3.5. Radiation Efficiency

The ability of a radio antenna to convert the received radio-frequency power into radiated power is quantified by its radiation efficiency. Material losses, dielectric properties, antenna design, and operating frequency all contribute to this efficiency.

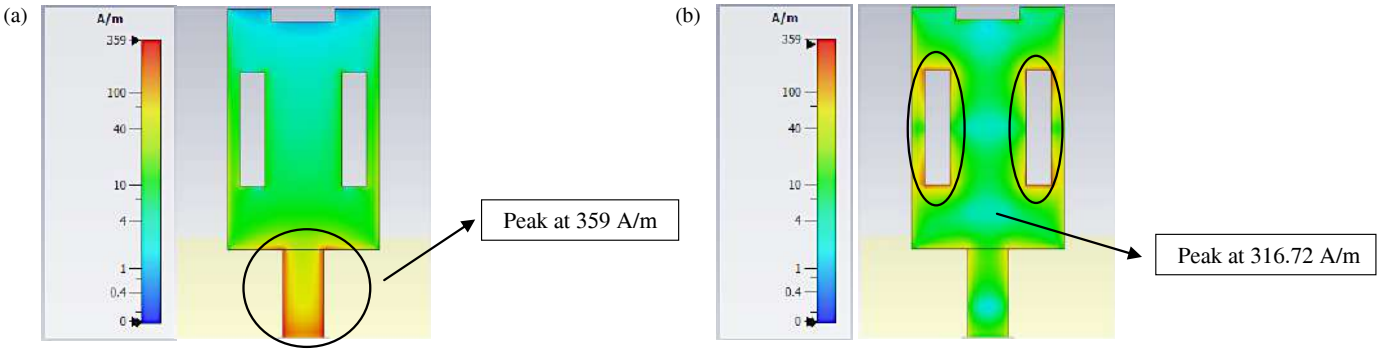

FIGURE 10. Current density distribution of the proposed antenna at different frequencies, (a) 3.5 GHz, (b) 17 GHz.

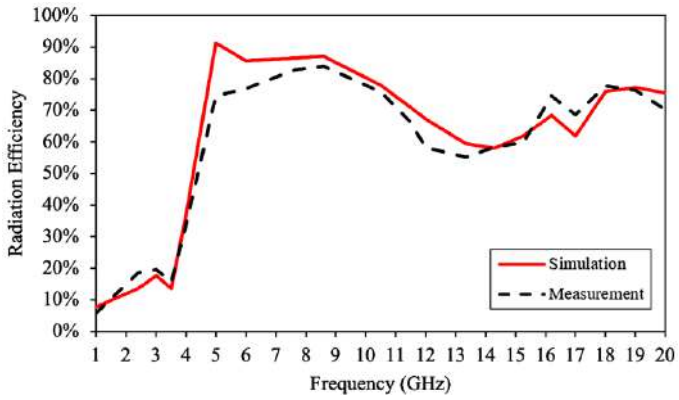

FIGURE 11. Radiation efficiency.

Antenna patch size at 3.5 GHz:

$$Area = L \times W = 26.3\,mm \times 20.5\,mm = 539.15\,mm^2$$

Antenna patch size at 17 GHz:

$$Area = L \times W = 9.5\,mm \times 6\,mm = 57\,mm^2$$

$$Compactness\ \% = \frac{Patch(3.5GHz) - Patch(17GHz)}{Patch(3.5GHz)} \times 100 = \frac{539.15 - 57}{539.15} \times 100 = 89.43\%$$

High radiation efficiency results in improved signal strength, range, and energy utilization, which is particularly crucial for applications with power constraints. The antenna's radiation efficiency, recorded at 77.69%, suggests potential effects from design limitations or material losses, as illustrated in Figure 11.

4. COMPARISON ANALYSIS

Table 2 compares the proposed antenna design with existing works in terms of key parameters such as frequency bands, dimensions, substrate materials, and return loss (S_{11}). While previous designs primarily focus on either compactness or bandwidth, our proposed antenna successfully integrates both without compromising performance.

Compared to [14] and [15], our design achieves a significantly smaller footprint of $13 \times 10\,mm^3$, making it one of the most compact antennas suitable for smartphone integration. Additionally, while [15] utilizes a much larger $140 \times 70 \times 6\,mm^3$ FR-4-based antenna for 5G operation, our antenna delivers comparable return loss performance at -19 dB (3.5 GHz) and -39 dB (17 GHz) within a significantly reduced form factor. Additionally, works like [16] and [18] explore multiband operation but often require larger substrates or additional components to optimize performance. Our antenna, however, effectively covers 5G, Ku-band, and K-band frequencies within a single compact structure, making it highly suitable for next-generation wireless applications. Furthermore, many existing designs use high-cost substrates like Rogers 5880 or RO4350B ([17] and [22]), whereas our design achieves excellent performance using an FR-4 substrate, which is cost-effective and widely available, making it more practical for commercial smartphone integration. These advantages collectively demonstrate that our proposed antenna provides an optimal trade-off among size, performance, and cost-effectiveness. It is well suited for 5G and satellite communication applications, making it a strong candidate for next-generation mobile devices.

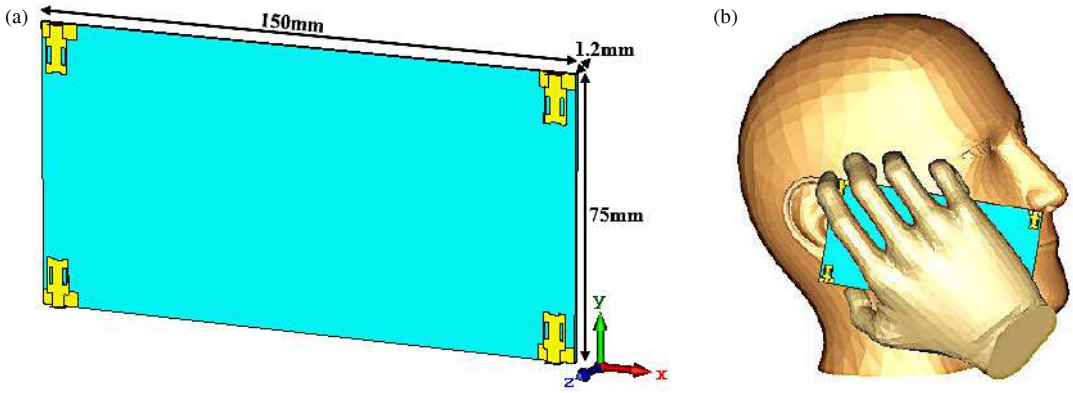

FIGURE 12. (a) A dielectric rear cover is depicted in the antenna diagram and (b) The antenna arrangement's configuration includes a hand and head model.

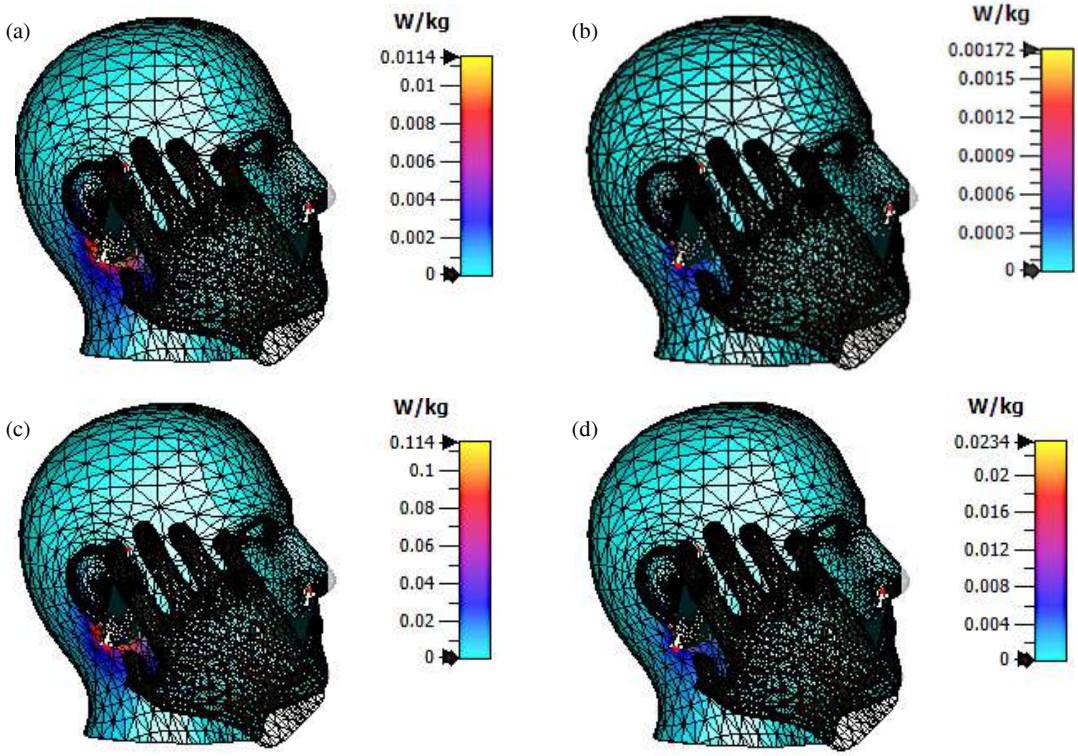

FIGURE 13. An evaluation of the simulated SAR for a multiband antenna configuration with a rear cover is conducted at 3.5 GHz, (a) 1 g and (b) 10 g. For 17 GHz, (c) 1 g and (d) 10 g measurements.

5. SPECIFIC ABSORPTION RATE (SAR)

5.1. Performance Impact of Radiation Properties and the User's Hand and Head

Specific Absorption Rate (SAR) quantifies the amount of electromagnetic (EM) radiation that the human body absorbs while using a mobile phone [25–29]. Predicting the SAR value of the proposed antenna design is crucial since it is mounted on the back cover. Regulatory agencies, such as the Federal Communications Commission (FCC) and International Commission on Non-Ionizing Radiation Protection (ICNIRP), have established SAR limits to ensure user safety. The FCC mandates a maximum SAR limit of 1.6 W/kg, averaged over 1 gram of tissue, while ICNIRP specifies a slightly higher limit of 2.0 W/kg, averaged over 10 grams of tissue. The antenna configuration, which includes the rear cover, is depicted in Figure 12(a).

Evaluating the SAR of the proposed antenna is critical, given its intended use in mobile devices. As depicted in Figure 12(b), a head phantom model is employed to measure the electromagnetic energy absorbed by the human skull. The antenna is oriented at a 65-degree angle relative to the negative vertical axis. As highlighted in [30], the separation distance between the antenna element and various body regions is a critical factor in determining the SAR value, which is a critical aspect of this analysis. Specifically, the antenna is replicated at a 5 mm distance from the human head phantom in this study, with a focus on the regions surrounding the ear and mandible. The orientation and location of the antenna have been meticulously opti-

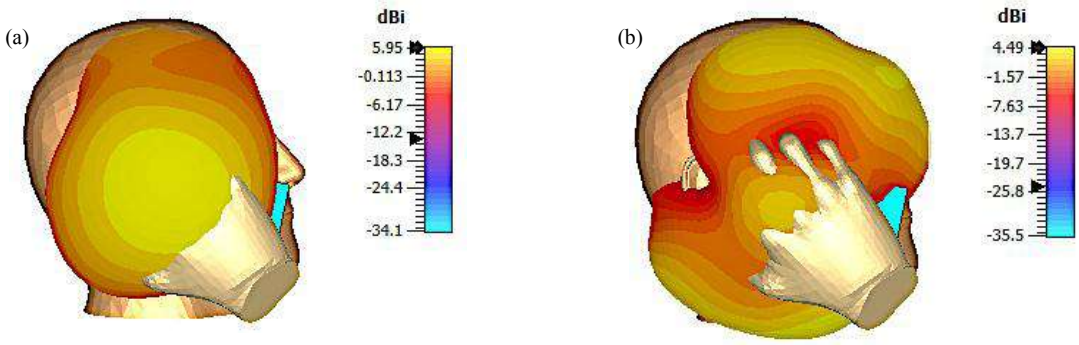

FIGURE 14. The 3D radiation characteristics of the proposed antenna in Talking Mode are influenced by interactions with the user's hand and head: (a) 3.5 GHz and (b) 17 GHz.

TABLE 2. Comparison for various related works.

Ref	Operating Frequency (GHz)	Antenna Size (mm^3)	Substrate Type	Gain (dBi)	Efficiency (%)	Return Loss S_{11}
[14]	2.45 3.5 5.2	$40 \times 35 \times 1.6$	FR-4	1.48 3.26 2.47	86 93.5 84.4	-15 -27 -14
[15]	3.5 5.5	$140 \times 70 \times 6$	FR-4	2.8 3.2	68 78	-23 -28
[16]	3.45 5.5	$17.5 \times 6 \times 0.2$	-	5.3 5.25	88.25 86.8	-24 -17
[17]	3.8 5.2 8	$24.8 \times 40 \times 0.254$	Rogers 5880	6.75	91	-18 -21 -22
[18]	0.7–0.96 1.6–5.5	$40 \times 15 \times 0.8$	FR-4	1.66 4.72	84 88	-23 -30
[19]	6.2	$20 \times 15 \times 1.6$	FR-4	3.5	-	-38
[20]	3–12.5	$15 \times 17 \times 1.548$	Rogers/RT5880	-0.5 and 2.2	40 and 80	-25 and -30
[21]	0.7–6	$80 \times 5 \times 4.5$	-	-	-	-
[22]	0.68-1 1.68–3 23.3–30.8	$6.5 \times 1.51 \times 1.2$	Rogers RO4350B	-	-	- - -40
[23]	3.5	$40 \times 52 \times 1.2$	FR-4	3.16	-	-39
This work	3.5 17	$13 \times 10 \times 1.6$	FR-4	-7.23 2.01	20.1 70	-19 -39

mised to guarantee a realistic representation of typical utilisation conditions. Moreover, a hand phantom model is situated at approximately 0.2 mm from the ground plane of the antenna.

As shown in Figure 13, the proposed antenna design demonstrates significantly lower SAR values, with measurements of 0.0114 W/kg (1 g tissue) and 0.00172 W/kg (10 g tissue) at 3.5 GHz, which are well below the FCC and ICNIRP safety limits. This ensures minimal radiation exposure and safe operation for long-term use in 5G-enabled smartphones. Additionally, the antenna configuration minimizes radiation towards the head and hand, optimizing user safety while maintaining high performance.

Figure 14 illustrates the antenna's radiation patterns, incorporating a human head model, a hand model, and a posterior antenna with a back cover.

A comparative analysis with existing antenna designs as highlighted in Table 3 shows that the proposed antenna achieves one of the lowest SAR values recorded for similar configurations. This improvement results from the strategic placement of the antenna on the device's rear cover, optimized positioning to reduce direct exposure, and enhanced radiation efficiency. By achieving such low SAR values, the proposed antenna aligns with global safety standards, ensuring a reliable and health-conscious solution for future wireless communication technologies.

TABLE 3. Comparison of SAR values for different antenna configurations.

References	Space (mm)	Power (dBm)	No. of elements	SAR. 1 g	SAR. 10 g
[25]	5	15	1	1.25	0.31
		20		NA	0.998
[26]	5	24	2	1.352	NA
[27]	NA	NA	NA	1.423	0.3
[28]	NA	24	8	NA	1.23
[29]	NA	NA	2	NA	0.36
[30]	5	15	2	1.18	0.963
		20		1.57	1.36
Suggested work	5	15	1	0.0116	0.00257

6. CONCLUSION

This study presents a compact and innovative multi-band microstrip patch antenna, specifically designed for 5G mobile devices. The antenna is highly suitable for various applications, including telecommunications, radar systems, and multimedia services, as it demonstrates efficient performance across the sub-6 GHz, Ku, and K-band frequency spectrums. Covering the 3.3–3.6 GHz and 15.6–20 GHz bands, it is tuned to resonant frequencies of 3.5 GHz and 17 GHz. Constructed on an FR4 substrate and employing a planar transmission line feed, the design combines exceptional performance with a highly compact footprint. The measured input reflection coefficient (S_{11}) and far-field patterns closely match the simulations, resulting in excellent return loss characteristics achieved through parametric optimization using CST software. The antenna's capabilities are further validated by its omnidirectional radiation patterns and maximum gain values of -2.8 dBi and 3.7 dBi. Its superior performance and compact design are demonstrated through a comparative evaluation, highlighting its potential as a versatile solution for next generation 5G communication systems.

ACKNOWLEDGEMENT

The authors would like to thank Universiti Teknikal Malaysia Melaka (UTeM) and the Ministry of Higher Education (MOHE) of Malaysia for supporting this project.

REFERENCES

[1] Jemaludin, N., A. J. A. Al-Gburi, R. H. Elabd, T. Saeidi, M. F. Akbar, I. M. Ibrahim, and Z. Zakaria, "A comprehensive review on MIMO antennas for 5G smartphones: Mutual coupling techniques, comparative studies, SAR analysis, and future directions," *Results in Engineering*, Vol. 23, 102712, 2024.

[2] Dayo, Z. A., M. Aamir, Z. Rahman, I. A. Khoso, M. M. Lodro, S. A. Dayo, P. Soothar, M. S. Pathan, A. J. A. Al-Gburi, A. A. Memon, and B. S. Chowdhry, "A novel low-cost compact high-performance flower-shaped radiator design for modern smartphone applications," *Micromachines*, Vol. 14, No. 2, 463, 2023.

[3] Barton, J. J., S. Zhai, and S. B. Cousins, "Mobile phones will become the primary personal computing devices," in *Seventh IEEE Workshop on Mobile Computing Systems & Applications (WMCSA'06 Supplement)*, 3–9, Orcas Island, WA, USA, Aug. 2005.

[4] Megahed, A. A., A. H. Hussein, A. J. A. Al-Gburi, and R. H. Elabd, "Compact wideband antenna array with DGS-based metamaterial for efficient smartphone communication and SAR reduction," *Progress In Electromagnetics Research B*, Vol. 110, 15–28, 2025.

[5] Abdullah Al-Gburi, A. J., "5G MIMO antenna: Compact design at 28/38 GHz with metamaterial and SAR analysis for mobile phones," *Przegląd Elektrotechniczny*, Vol. 2024, No. 4, 171, 2024.

[6] Fortunati, L., "The smartphone between the present and the future: Five changes," *Mobile Media & Communication*, Vol. 11, No. 1, 19–24, Oct. 2022.

[7] Han, Q. and D. Cho, "Characterizing the technological evolution of smartphones: Insights from performance benchmarks," in *Proceedings of the 18th Annual International Conference on Electronic Commerce: E-Commerce in Smart connected World*, 1–8, 2016.

[8] Thakur, E., A. Gupta, M. K. Abdulhameed, A. D. Khaleel, and A. J. A. Al-Gburi, "Microstrip antenna with two elements and defected ground structure for 5G mobile applications at 28/38 GHz," *Progress In Electromagnetics Research C*, Vol. 146, 177–185, 2024.

[9] Elabd, R. H. and A. J. A. Al-Gburi, "Low mutual coupling miniaturized dual-band quad-port MIMO antenna array using decoupling structure for 5G smartphones," *Discover Applied Sciences*, Vol. 6, No. 4, 189, 2024.

[10] Elabd, R. H. and A. J. A. Al-Gburi, "Super-compact 28/38 GHz 4-port MIMO antenna using metamaterial-inspired EBG structure with SAR analysis for 5G cellular devices," *Journal of Infrared, Millimeter, and Terahertz Waves*, Vol. 45, No. 1, 35–65, 2024.

[11] Wang, H., "Overview of future antenna design for mobile terminals," *Engineering*, Vol. 11, 12–14, Apr. 2022.

[12] Rashmitha, R., N. Niran, A. A. Jugale, and M. R. Ahmed, "Microstrip patch antenna design for fixed mobile and satellite 5G communications," *Procedia Computer Science*, Vol. 171, 2073–2079, 2020.

[13] Elabd, R. H. and A. J. A. Al-Gburi, "Ultra-compact 4-port MIMO antenna with defected ground structure and SAR analysis for 28/38 GHz 5G mobile devices," *Journal of Electromagnetic Waves and Applications*, Vol. 38, No. 9, 1000–1025, 2024.

[14] Shah, I. A., S. Hayat, I. Khan, I. Alam, S. Ullah, and A. Afridi, "A compact, tri-band and 9-shape reconfigurable antenna for WiFi, WiMAX and WLAN applications," *International Journal of Wireless and Microwave Technologies*, Vol. 6, No. 5, 45–53, Sep. 2016.

[15] Khan, A., A. Wakeel, L. Qu, and Z. Zahid, "Dual-band 8×8 MIMO antenna with enhanced isolation and efficiency for 5G smartphone applications," *AEU — International Journal of Electronics and Communications*, Vol. 163, 154600, May 2023.

[16] Kulkarni, J. S., "An ultra-thin, dual band, Sub 6 GHz, 5G and WLAN antenna for next generation laptop computers," *Circuit World*, Vol. 46, No. 4, 363–370, Apr. 2020.

[17] Saeidi, T., I. Ismail, S. Noghanian, A. R. H. Alhawari, Q. H. Abbasi, M. A. Imran, M. Y. Zeain, and S. M. Ali, "High gain triple-band metamaterial-based antipodal Vivaldi MIMO antenna for 5G communications," *Micromachines*, Vol. 12, No. 3, 250, Feb. 2021.

[18] An, Z. and M. He, "A simple planar antenna for sub-6 GHz applications in 5G mobile terminals," *Applied Computational Electromagnetics Society Journal (ACES)*, Vol. 35, No. 1, 10–15, 2020.

[19] Singh, T., P. Sharma, S. Tripathi, and V. S. Tripathi, "Elliptical multi orbital truncated flexible patch antenna using PDMS substrate for sub 6 GHz applications," *Defence Science Journal*, Vol. 74, No. 4, 546–551, Jul. 2024.

[20] Al-Gburi, A. J. A., Z. Zakaria, M. Palandoken, I. M. Ibrahim, A. A. Althuwayb, S. Ahmad, and S. S. Al-Bawri, "Super compact UWB monopole antenna for small IoT devices," *Computers, Materials & Continua*, Vol. 73, No. 2, 2785–2799, 2022.

[21] Alja'afreh, S., A. Khalfalla, and A. Omar, "Universal antenna with a small non-ground portion for smartphone applications," *International Journal on Communications Antenna and Propagation (IRECAP)*, Vol. 9, No. 4, 292, Aug. 2019.

[22] Xia, X., F. Wu, C. Yu, Z. Jiang, J. Xu, S.-Y. Tang, Z. Wang, Y. Yao, and W. Hong, "Millimeter-Wave and sub-6 GHz aperture-shared antenna and array for mobile terminals accessing 5G/6G-enabled IoT scenarios," *IEEE Internet of Things Journal*, Vol. 11, No. 10, 18 808–18 823, 2024.

[23] Kartikasari, G., M. P. K. Praja, and S. Romadhona, "Design of rectangular patch microstrip antenna with defected ground structure method at 3.5 GHz frequency for 5G technology," *Journal of Information Technology and Its Utilization*, Vol. 6, No. 2, 79–85, Dec. 2023.

[24] Andrews, C. J. M., A. S. K. Narayanan, and A. M. Sunil, "Compact metamaterial based antenna for 5G applications," *Results in Engineering*, Vol. 24, 103269, Dec. 2024.

[25] Lak, A., Z. Adelpour, H. Oraizi, and N. Parhizgar, "Design and SAR assessment of three compact 5G antenna arrays," *Scientific Reports*, Vol. 11, No. 1, 21265, Oct. 2021.

[26] Farooq, U. and G. M. Rather, "A miniaturised Ka/V dual band millimeter wave antenna for 5G body centric network applications," *Alexandria Engineering Journal*, Vol. 61, No. 10, 8089–8096, Oct. 2022.

[27] Zada, M., I. A. Shah, and H. Yoo, "Integration of sub-6-GHz and mm-wave bands with a large frequency ratio for future 5G MIMO applications," *IEEE Access*, Vol. 9, 11 241–11 251, 2021.

[28] Elabd, R. H. and A. J. A. Al-Gburi, "Super-compact 28/38 GHz 4-port MIMO antenna using metamaterial-inspired EBG structure with SAR analysis for 5G cellular devices," *Journal of Infrared Millimeter and Terahertz Waves*, Vol. 45, 35–65, 2024.

[29] Khan, J., D. A. Sehrai, and U. Ali, "Design of dual band 5G antenna array with SAR analysis for future mobile handsets," *Journal of Electrical Engineering & Technology*, Vol. 14, 809–816, Mar. 2019.

[30] Elabd, R. H. and A. J. A. Al-Gburi, "SAR assessment of miniaturized wideband MIMO antenna structure for millimeter wave 5G smartphones," *Microelectronic Engineering*, Vol. 282, 112098, Oct. 2023.